Spin reorientation in Dy-based high-entropy oxide perovskite thin films

Maria Cocconcelli,[1,*] Duncan Miertschin,[2] Balaram Regmi,[2] Davis Crater,[2] Federico Stramaglia,[3] Lide Yao,[4] Riccardo Bertacco,[1] Cinthia Piamonteze,[3] Sebastiaan van Dijken,[5] and Alan Farhan[2,†]

[1]*Dipartimento di Fisica, Politecnico di Milano, 20133 Milano, Italy*
[2]*Department of Physics, Baylor University, One Bear Place, Waco, Texas 76798, USA*
[3]*Paul Scherrer Institute, Forschungsstrasse 111, 5232 Villigen PSI, Switzerland*
[4]*OtaNano-Nanomicroscopy Center, Aalto University School of Science, P.O. Box 15100, FI-00076 Aalto, Finland*
[5]*Department of Applied Physics, Aalto University School of Science, P.O. Box 15100, FI-00076 Aalto, Finland*

(Received 31 December 2023; revised 29 February 2024; accepted 27 March 2024; published 15 April 2024)

We present a study on the structural and magnetic properties of thin films of the high entropy perovskite $Dy(Fe_{0.2}Mn_{0.2}Co_{0.2}Cr_{0.2}Ni_{0.2})O_3$ (Dy5BO). An element-sensitive investigation was performed using synchrotron-based x-ray absorption spectroscopy, employing x-ray magnetic circular and linear dichroism. The results reveal that the moments residing on the 3*d* transition metal ions and the rare-earth Dy ions produce a saturation magnetization one order of magnitude larger than any previously studied high-entropy oxide perovskite. Employing temperature-dependent x-ray magnetic linear dichroism, we see clear features of a spin reorientation at the Mn and Fe sites, occurring around 18 K, likely driven by the interaction of the corresponding transition metal ions and Dy.

DOI: 10.1103/PhysRevB.109.134422

I. INTRODUCTION

Over the past few decades, a considerable amount of research has been devoted to rare-earth transition metal oxide perovskites, denoted by the general formula ABO_3, where *A* represents a rare-earth ion and *B* denotes a 3*d* transition metal ion, due to their intriguing multiferroic properties and functionalities [1,2]. Recently, a new class of materials known as high-entropy oxides (HEOs) has emerged [3,4]. In these materials, the presence of a large number of cations present at the same lattice site in equiatomic proportions significantly enhances the configurational entropy. This leads to single-crystal stabilization, notwithstanding the radii, charge, atomic mass, and magnetic properties of the ions, and enables for many design possibilities [5]. HEOs hold promise as potential sources for the realization of large-*k* dielectrics [6], multifunctional semiconductors [7], relaxor ferroelectrics [8], and materials with low thermal conductivity [9].

The entropy-driven stabilization concept has been applied to the development of rare-earth transition metal oxide perovskites, resulting in the emergence of a class of complex oxides referred to as high entropy oxide perovskites (HEOPs). These materials, which can be synthesized in both bulk [10] and thin-film configurations [5,11], exhibit a wide range of intriguing properties, including high magnetoresistance [12], metal-insulator transitions, thermoelectric properties [13], and multifunctional behavior [7]. Due to the immense design potential entropy-driven stabilization and the interplay of lattice and orbital degrees of freedom, HEOPs have been identified as ideal candidates for the study and development of multifunctional properties. It has also been shown that the growth of thin HEOP films, achieved through methods like pulsed laser deposition (PLD), is especially interesting as it facilitates single-crystal stabilization mechanisms that extend beyond the entropy-driven process due to its near instantaneous quench time. Such mechanisms encompass substrate-driven stabilization, oxygen pressure, growth temperature, and laser fluence. This growth-induced stabilization allows the realization of HEOP thin films that may not be feasible in the bulk.

Our recent element-sensitive x-ray absorption spectroscopy study on $Tb(Fe_{0.2}Mn_{0.2}Co_{0.2}Cr_{0.2}Ni_{0.2})O_3$ (Tb5*B*O) [14] and $Lu(Fe_{0.2}Mn_{0.2}Co_{0.2}Cr_{0.2}Ni_{0.2})O_3$ (Lu5*B*O) [15] shed light on the diverse magnetic behavior exhibited by HEOPs. In the case of Tb5*B*O thin films, analysis revealed the presence of long-range ferromagnetic order, likely driven by an enhanced presence of Co^{2+} [14]. Conversely, the investigation of Lu5*B*O thin films demonstrated dominant antiferromagnetic ordering below 100 K marked by a significant reduction in the presence of Co^{2+}, possibly due to the lack of tensile strain and the relaxed nature of Lu5*B*O thin films grown on $SrTiO_3$ (STO) (001) substrates [15]. The intricate magnetic interactions in these systems are highly influenced by the collective electronic configuration of the transition metal ions, which, in turn, are determined by the specific rare-earth ion occupying the *A* sublattice. One of the fascinating phenomena that is driven by *A*-site ordering in perovskites is that of spin reorientations, for example in $DyFeO_3$ [16,17]. The spin reorientation transition in orthoferrites is important for new applications and it provides insight into magnetic interactions and phase transitions [18].

These previous results on $DyFeO_3$ raise the question whether spin reorientation transitions can occur in Dy-based HEOP thin films, despite the disorder and randomness of the transition metal ions occupying the *B* sublattice.

*maria.cocconcelli@polimi.it
†alan_farhan@baylor.edu

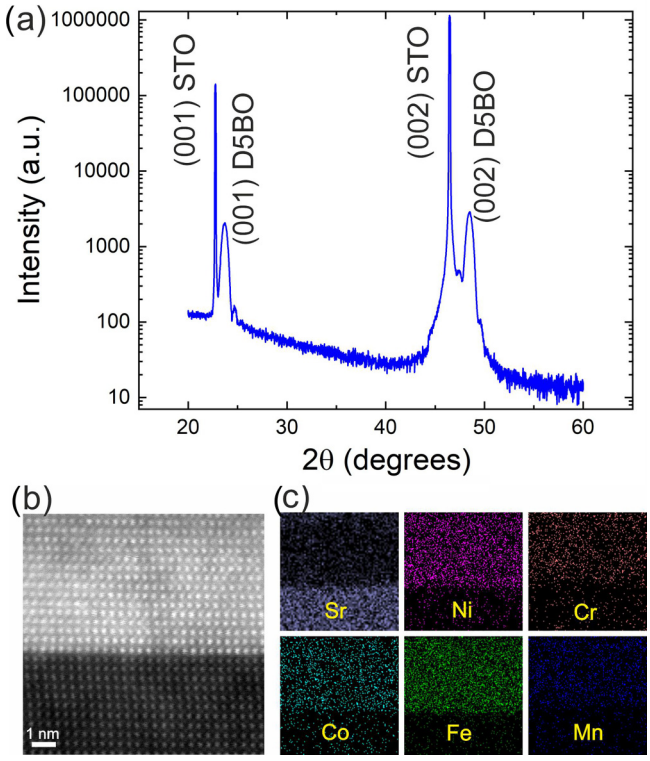

FIG. 1. (a) XRD θ-2θ scan of a 12 nm thick Dy5*B*O film grown on a (001)-oriented STO substrate. The film displays good crystal quality without any secondary phases. (b) STEM image of the film along the [100] direction, showing epitaxial growth. (c) EDX images recorded in the same area as (b), revealing an isotropic and random distribution of the transition metal elements.

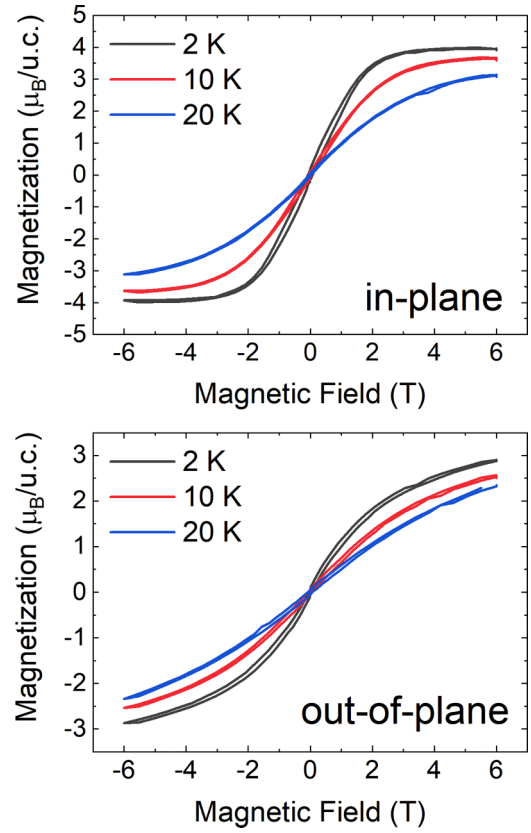

FIG. 2. SQUID-VSM magnetic hysteresis loops measured at different temperature on a 12 nm thick Dy5*B*O film, with (a) an in-plane magnetic film and (b) an out-of-plane magnetic field.

To address this question, we report the growth of $Dy(Fe_{0.2}Mn_{0.2}Co_{0.2}Cr_{0.2}Ni_{0.2})O_3$ thin films on STO (001) substrates. In addition to structural and macroscopic magnetic characterization, we provide an x-ray absorption spectroscopy (XAS) study, employing x-ray magnetic circular and linear dichroism (XMCD and XMLD) at the $L_{2,3}$ absorption edges of all five transition metal elements within the perovskite *B* block and we investigate the occurrence of a spin reorientation.

II. RESULTS AND DISCUSSION

A. Experimental methods

Thin films of Dy5*B*O were grown by pulsed laser deposition (PLD) on TiO_2-terminated STO (001) substrates, using a KrF excimer laser ($\lambda = 248$ nm) with a repetition rate of 5 Hz and fluence of 1.52 J/cm^2. Optimal growth conditions were obtained for a substrate temperature of 820 °C, a target-substrate distance of 5.5 cm, and an oxygen partial pressure of 0.14 mbar. We used 14 000 pulses to deposit thin films with a thickness of 12 nm. Following the growth, the films were cooled to 260 °C under an oxygen pressure of 100 mbar, at a cooling rate of 4 °C/min.

The structural properties of the films were analyzed by x-ray diffraction (XRD), using a Rigaku Smartlab high-resolution four-circle x-ray diffractometer in reduced fluorescence mode. The composition and microstructural properties of the films were characterized using a JEOL 2200FS scanning transmission electron microscope (STEM) equipped with an electron dispersive x-ray spectrometer (EDX). We recorded magnetic hysteresis loops utilizing a Quantum Design superconducting quantum interference device (SQUID-VSM) magnetometer. Element-sensitive x-ray absorption spectroscopy (XAS) by total electron yield (TEY) was conducted at the XTreme beamline of the Swiss Light Source [19]. X-ray circular and linear dichroism (XMCD and XMLD) techniques were employed at the $L_{2,3}$ edges [20,21] of the five transition metal elements, and at the $M_{4,5}$ edge of Dy.

B. Structural, compositional, and magnetic characterization

The XRD θ-2θ scan depicted in Fig. 1(a) illustrates that the Dy5BO film exhibits a (001)-oriented crystalline structure, with an out-of-plane lattice parameter of $c = 3.761$ Å. Because the STO substrate has lattice parameters $a = b = c = 3.905$ Å, the Dy5BO film experiences strong tensile strain. STEM imaging reveals a clean interface between the substrate and the film, as shown in Fig. 1(b). Compositional analysis by EDX shows that the transition metal elements are uniformly distributed throughout the investigated area, without clustering [Fig. 1(c)].

The macroscopic magnetic properties of the Dy5BO film were subjected to SQUID-VSM magnetometry. Figures 2(a) and 2(b) depict hysteresis loops of a 12 nm thick Dy5BO film, measured at 2 K, 10 K, and 20 K, for both in-plane

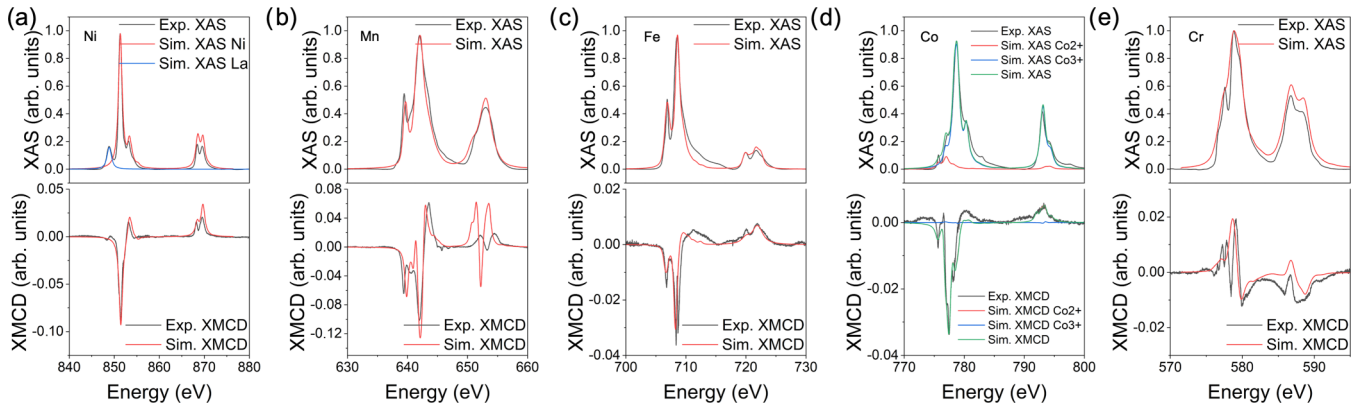

FIG. 3. XAS spectra (upper panel) and XMCD spectra (lower panel) of (a) Ni, (b) Mn, (c) Fe, (d) Co, and (e) Cr recorded at 2.5 K. The measurements are conducted in the out-of-plane geometry with a 6 T field.

(a) and out-of-plane (b) magnetic field orientations. The in-plane hysteresis loop at 2 K exhibits a small opening, and it saturates around 2 T. The saturation magnetization is close to 4.0 μ_B/u.c., which is almost an order of magnitude larger than previously studied HEOPs [10,14,15]. The magnetic response softens with increasing temperature [see red and blue curves in Fig. 2(a)]. The hysteresis curves recorded with out-of-plane magnetic field show a small opening and the magnetization does not saturate at 6 T. Furthermore, the hysteresis loops do not exhibit the distinctive "wasp shape," which has been observed for Tb5*B*O [14], Lu5*B*O [15], and La5*B*O [10]. Measurements of the in-plane magnetization versus temperature after cooling under zero or applied field are available in the Supplemental Material [22].

C. XMCD spectroscopy and sum rule analysis

Element-sensitive XMCD spectroscopic measurements were carried out at the $L_{2,3}$ edges of the five transition metals elements in the *B* block of Dy5*B*O (Ni, Fe, Cr, Mn, Co) by subtracting the spectra obtained using x-rays with circular right (c^+) and circular left (c^-) polarization. The measurements were carried out at 2.5 K, 25 K, 50 K, 75 K, 100 K, and 125 K in both grazing geometry, with the x-rays impinging on the sample at a grazing angle of 30°, and the out-of-plane geometry, with the incoming x-rays normal to the film surface. The magnetic field is always applied parallel to the incoming x-rays in XMCD measurements. Figure 3 shows normalized XAS and XMCD spectra collected at 2.5 K in the out-of-plane geometry with a 6 T field. These spectra are fitted to calculations based on ligand field theory in CTM4XAS 5.5 software [23]. The calculations are executed by first selecting the electronic configuration and the site symmetry of the absorbing element. Then, different parameters are tuned, drawing comparisons from the literature [24–28], including the crystal field spitting, to accommodate the octahedral symmetry, spin-orbit coupling, and the reduction of Slater integrals, and to account for screening and mixing effects. Lifetime effects are considered by introducing an intrinsic broadening of each edge, which enters the calculation as the convolution of the calculated spectra with a Lorentzian [29]. Moreover, to account for experimental broadening effects, an additional Gaussian broadening of 0.2 eV is applied. The calculated spectra are then shifted by −2.15 eV in the photon energy to match the energy scale of the experimental spectra.

The detailed values of the parameters employed in the calculations are provided in the Supplemental Material [22]. By fitting the experimentally recorded spectra, we conclude that the measured data can be replicated with an octahedral environment, as expected in a perovskite. Additionally, we determine the oxidation states of the transition metals in the Dy5*B*O film, which are Ni^{2+}, Fe^{3+}, Cr^{3+}, and Mn^{4+}. The XAS and XMCD spectra of Co reveal the coexistence of Co^{2+} and Co^{3+} oxidation states, constituting approximately 13% and 87% of the total composition, respectively. Despite the higher concentration of Co^{3+} compared to Co^{2+}, the XMCD spectra primarily reflects the contribution from high-spin Co^{2+}, due to the negligible signal generated by Co^{3+}, indicating its low-spin state. The concentration of Co^{2+} compared to Co^{3+} in the Dy5*B*O sample presents an intermediate situation between the findings observed in Tb5*B*O (23%) and Lu5*B*O (2%) [14,15]. The peaks observed at 848 eV in the XAS spectra of Ni and at 782 eV and 797 eV in the XAS spectra of Co are indicative of the presence of low concentrations of La and Ba impurities, respectively. Based on the relative intensity of these peaks, it can be estimated that the relative content of La with respect to Ni is approximately 3%, while the relative impurity content of Ba with respect to Co is less than 1%.

Notably, Cr XMCD is opposite in sign with respect to the XMCD signal measured for other transition metal elements, suggesting that the magnetic moments of Cr have a magnetic response that opposes that of all other transition metal ions [30,31]. The substantial compositional disorder inherent in high-entropy perovskites is known for inducing spin frustration. For instance, in La-based HEOP thin films, Cr exhibited a disappearing XMCD contrast attributed to compensating competing ferro- and antiferromagnetic interactions [32]. Therefore, the notable XMCD contrast observed in Cr within Dy5*B*O films implies that these competing interactions may not completely cancel each other out in this system.

The XAS and XMCD spectra of the Dy5*B*O film depict a scenario largely consistent with that observed for Tb5*B*O [14], with the most notable difference being the concentration of Co^{2+} ions and the antiparallel alignment of the Cr magnetic moment. However, the saturation magnetization of Dy5*B*O

TABLE I. XMCD sum rule analysis for the elements in the Dy5*B*O film obtained from XAS and XMCD spectra collected at 2.5 K in the out-of-plane x-ray configuration under the application of a 6 T field.

Element (corr. Factor)	Number of holes	m_S (μ_B)	m_L (μ_B)	m_L/m_S
Ni (0.92)	2	−0.33(7)	−0.12(2)	0.39
Mn (0.59)	7	−1.7(2)	0.034(4)	−0.02
Co (0.89)	3	−0.26(1)	−0.032(6)	0.12
Fe (0.68)	5	−0.24(1)	0.0039(7)	−0.01
Dy	5	−1.07(5)	−1.7(5)	1.6

is almost an order of magnitude larger than that of Tb5*B*O. To understand the difference in saturation magnetization, we proceed to estimate the spin (m_S), orbital (m_L), and total magnetic moment ($m_L + m_S$) per average transition metal ion. To evaluate the magnetic moments, we apply the XMCD sum rule analysis [33–35] to the XAS and XMCD spectra. Sum rules can be applied when the L_2 and L_3 are well separated; for early transition metal ions where this condition is not met, significant correction factors must be considered [36]. Consequently, sum rules are not applied to Cr, and its magnetic moment is estimated to be $-0.05\ \mu_B$ based on comparison with [30].

We determined the spin, orbital, and total magnetic moment per average transition metal ion by applying formula (S1) and (S2) reported in the Supplemental Material [22] on the XMCD signal collected at 2.5 K in the out-of-plane measurement geometry, with a 6 T field. The results of the sum rule analysis are summarized in Table I. Mn exhibits the highest m_S with a value of $-1.71\ \mu_B$, while Ni shows the highest ratio of orbital magnetic moment (m_L) to spin magnetic moment (m_S) with a ratio of 0.39. To probe the in-plane magnetic moments, XAS and XMCD spectra were also recorded with x-ray incident at a 30° grazing angle and a 6 T field. Table II summarizes the sum rule analysis of these measurements. For both measurement configurations, the extracted spin and orbital magnetic moments are within experimental error. Averaging the magnetic moments of all transition metal ions in the Dy5*B*O unit cell gives 0.51 $\mu_B/u.c.$, which does not fully account for the 2.8 $\mu_B/u.c.$ measured by SQUID-VSM magnetometry at an equivalent field (Fig. 2). Therefore, we recorded XMCD spectra at the $M_{4,5}$ edge of Dy, using the out-of-plane geometry and a 6 T field. By applying already established sum rules [33,34,37], which are given in the Supplemental Material [22], we attained the results presented in Table I. We find that the Dy ions exhibit a substantial magnetic moment, which, together with the magnetic moment of the transition metal ions, adds up to 3.4 $\mu_B/u.c.$. This result derived from element specific XMCD measurements is in reasonable agreement with the macroscopic SQUID-VSM data in Fig. 2. Sum rule integrations for the grazing and out-of-plane geometry are given in the Supplemental Material [22].

D. Element sensitive magnetometry

To investigate the individual contribution of each transition metal element to the overall magnetic response of the Dy5*B*O film, further element-sensitive XMCD hysteresis loops were acquired at the L_3 edges in the 5*B* block. The measurements, shown in Fig. 4, were conducted in both the grazing and out-of-plane configurations by sweeping the magnetic field between −6 T and 6 T in steps of 0.1 T. The XMCD loops were recorded at 2.5 K and 25 K. Ni exhibits the most prominent opening in the hysteresis loop. The opening is more pronounced in the grazing configuration and it diminishes with increasing temperature. The XMCD measurements on Mn, Co, and Fe show smaller hysteresis and reduced signal in saturation. Cr shows a small hysteresis in the grazing configuration at 2.5 K but not in the out-of-plane measurement. Corresponding to the recorded Cr XCMD signal, its hysteresis loop exhibits an inverted trend compared to the other transition metals, reflecting its opposite response to an external magnetic field. By comparing the hysteresis loops obtained with a grazing and out-of plane magnetic field we conclude that the easy axis of the magnetization lies in the plane, which is consistent with the SQUID-VSM magnetometry measurements depicted in Fig. 2. The magnetic behavior of the transition metals, as illustrated by the XMCD hysteresis curves, closely mirrors that observed in Tb5*B*O thin films [14], which is noteworthy considering the contrasting overall magnetic behavior of the two films in terms of anisotropy and intensity of the magnetic moment.

E. X-ray magnetic linear dichroism and spin reorientation

To investigate possible antiferromagnetic contributions to the overall ordering in Dy5*B*O, we conducted

TABLE II. XMCD sum rule analysis for the elements in the Dy5*B*O film obtained from XAS and XMCD spectra collected at 2.5 K in the grazing x-ray configuration under the application of a 6 T field.

Element (corr. Factor)	Number of holes	m_S (μ_B)	m_L (μ_B)	m_L/m_S
Ni (0.92)	2	−0.59(1)	−0.098(7)	−0.16
Mn (0.59)	7	−1.3(1)	−0.11(8)	−0.08
Co (0.89)	3	−0.16(1)	−0.027(6)	0.16
Fe (0.68)	5	−0.50(1)	0.016(3)	−0.03

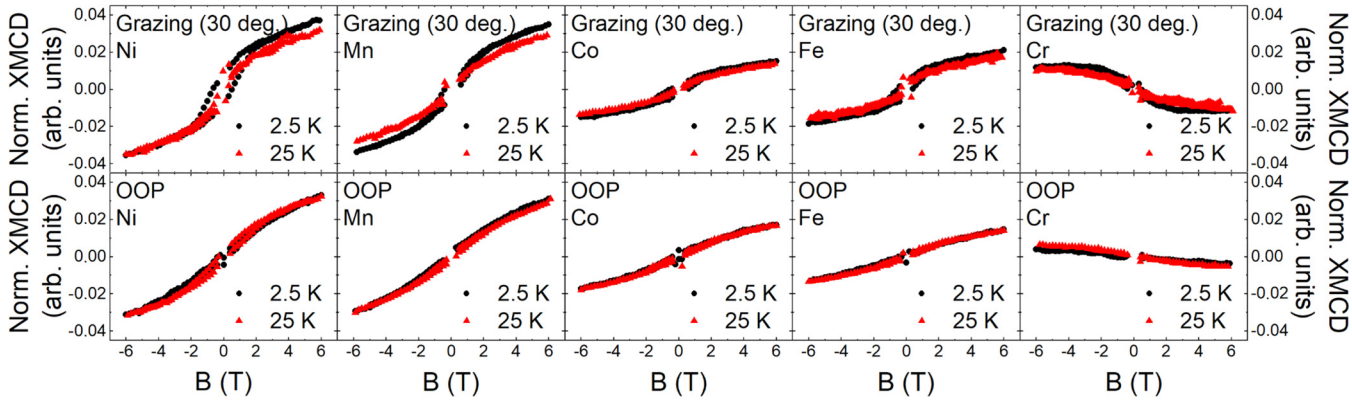

FIG. 4. XMCD loops collected at the L_3 edge of the transition metal elements in the 5*B* block of the Dy5*B*O film. The loops were collected at 2.5 K and 25 K, in both the grazing and out-of-plane geometry by sweeping the magnetic field between −6 T and 6 T in 0.1 T steps.

element-sensitive x-ray magnetic linear dichroism (XMLD) spectroscopy at the $L_{2,3}$ edge for the 5*B* transition metal elements. The measurements were performed with the x-ray impinging on the sample at a grazing angle of $\Theta = 30^\circ$ and zero magnetic field. XAS spectra were recorded with *s*- and *p*-polarized x-rays, as shown in Fig. 5(a), and XMLD was obtained by subtracting the spectra measured with *p*-polarized x-rays form the spectra measured with *s*-polarized x-rays. XAS with linearly polarized x-rays is sensitive to the alignment of the antiferromagnetic spin axis and the incident polarization. The sign of the XMLD signal in our measurements thus indicates whether the antiferromagnetic spins are oriented in-plane or out-of-plane in the Dy5*B*O film [38–40]. If the higher energy peak at the L_2 edge of a transition metal [the D peak in Fig. 5(b)] exhibits higher intensity, the antiferromagnetic spins are oriented parallel to the x-ray *s*-polarization [38,41]. To distinguish the antiferromagnetic contributions to the XMLD signal from natural dichroism caused by crystal-field-induced charge anisotropy, we measured XMLD spectra as a function of temperature. As an example, Fig. 5(c) shows the XMLD spectra recorded at the L_2 edge of Fe for different temperatures. The sign reversal of the XMLD signal [Figs. 5(c) and 5(d)] between 18 and 25 K indicates a reorientation of the antiferromagnetic spin axis from in plane at low temperature to out of plane at higher temperature [19]. A similar temperature-induced spin-reorientation transition is also measured for Mn [Fig. 5(f)]. The compositional disorder on the *B* site gives rise to various local environments, which may result in not all Mn and Fe ions undergoing this spin reorientation. The temperature dependence of the XMLD signal of Cr is different, showing a strong decline from around 25 K [Fig. 5(h)]. The XMLD signal of Ni does not show a clear variation with temperature [Fig. 5(e)]. In contrast, the XMLD signal for Co exhibits a peak at around 18 K, before it remains constant at higher temperature, a behavior that seems to correlate to the observed spin reorientation at the Fe and Mn sites.

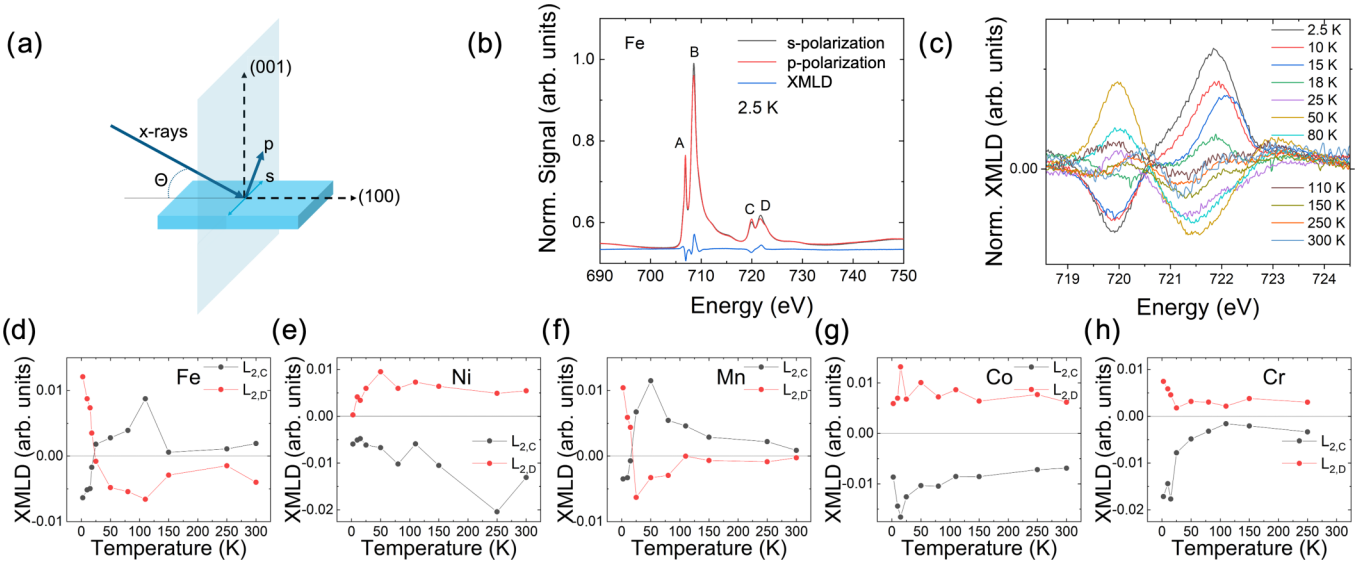

FIG. 5. (a) Measurement geometry for the recording of XMLD spectra. The incident angle of x-rays is $\Theta = 30^\circ$. (b) Normalized XAS spectra recorded with *s*- and *p*-polarized x-rays. (c) XMLD spectrum (blue curve) obtained at 2.5 K at the Fe L_2 edge. Panels (d)–(h) show the trend with temperature of the XMLD L_2 peaks C and D, respectively, for (d) Fe, (e) Ni, (f) Mn, (g) Co, and (h) Cr. The spectra are obtained at zero-field conditions.

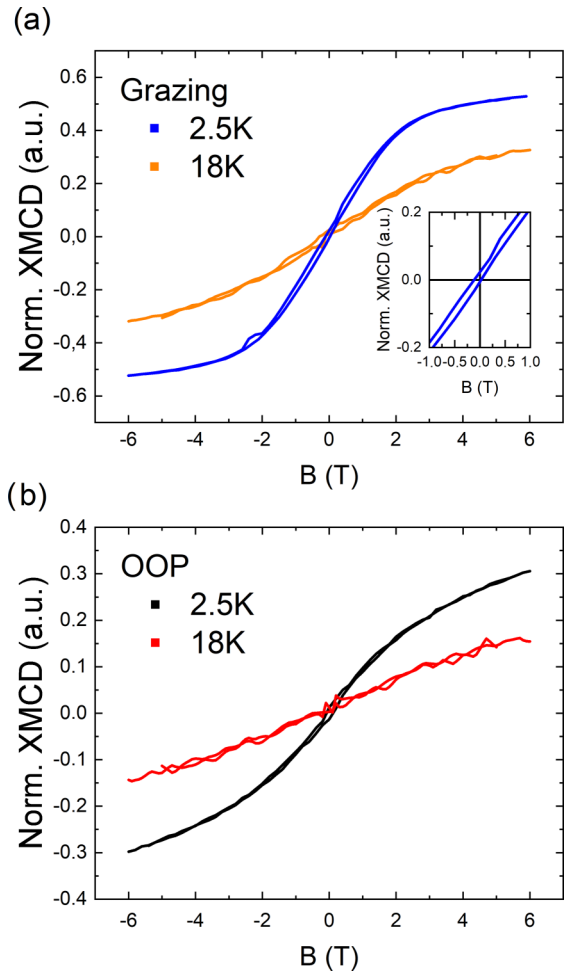

FIG. 6. XMCD hysteresis loops collected at the M_5 edge of Dy. The loops recorded at 2.5 K and 18 K in both (a) the grazing and (b) out-of-plane x-ray geometry.

F. Dysprosium XMCD hysteresis loops

Spin reorientation transitions in rare-earth orthoferrites such as $DyFeO_3$ are known to be driven by the the Dy anisotropy, the Dy-Fe interaction and the corresponding interatomic distances [17,42]. Bulk $DyFeO_3$ orders below 645 K into a G-type antiferromagnetism with antiparallel nearest-neighbor Fe moments [43]. Strong spin-orbit coupling results in spin canting and the emergence of weak ferromagnetism, which transitions to a C-type antiferromagnetism below a spin-reorientation transition that is driven by an increasing role of Dy-Fe interactions.

Considering the suspected important role of the Dy magnetic anisotropy in the observed spin reorientation in Dy5*B*O, we recorded XMCD hysteresis loops at the Dy M_5 edge at 2.5 K and 18 K, both with the magnetic field applied at grazing incidence and out of plane. An interesting first impression is that the 2.5 K measurements show similarities to the macroscopic SQUID-VSM measurements, with the grazing XMCD hysteresis loop featuring a hysteresis with a small opening [see inset in Fig. 6(a)] and near saturation at 6 T, while the out-of-plane XMCD hysteresis appears to be weaker and mostly closed [see black curve in Fig. 6(b)] and remaining far from saturation at 6 T. At 18 K, Dy5*B*O features a paramagnetic linear form for the out-of-plane XMCD hysteresis measurement [red line in Fig. 6(b)], while the grazing measurement at 18 K exhibits a nearly linear remnant hysteresis [orange line in Fig. 6(a)]. All together, these results reveal that long-range order of the Dy moments disappears above 18 K, which coincides with the spin reorientation transition temperature extracted from temperature-dependent XMLD measurements. It suggests that the emergence of ordered Dy moments and their interaction with the Fe moments and Mn moments is a likely driver of the aforementioned spin reorientation. It is interesting to note that the shape of the Dy XMCD hysteresis loops closely resemble the macroscopic hysteresis curves measured with SQUID magnetometry (compare Fig. 6 with Fig. 2), thus further confirming that Dy is the dominant contributor to the overall magnetic response in Dy5*B*O.

III. SUMMARY AND OUTLOOK

In summary, we conducted a comprehensive investigation of a spin reorientation occurring in Dy5*B*O thin films grown on STO (001) substrates, using magnetometry and element-sensitive x-ray absorption spectroscopy. The magnetic moment per unit cell of the film is stronger compared to other high-entropy perovskite thin films, which can be attributed to the substantial moment of Dy, as estimated through the sum rule analysis. Additionally, transition metal XMCD hysteresis loops in both Tb5*B*O and Dy5*B*O exhibit strong similarities, while their macroscopic magnetic responses recorded via SQUID magnetometry differ significantly. Moreover, the Dy XMCD hysteresis loop bears a striking resemblance to the SQUID magnetometry curve for Dy5*B*O. Taken together, these observations strongly suggest that the observed magnetic anisotropy in Dy5*B*O is driven by Dy ordering. Furthermore, our examination through XMLD supported with XMCD hysteresis loops revealed a spin-reorientation transition for Mn and Fe, likely linked to a Dy anisotropy emerging at temperatures below 18 K. Interestingly, compared to other HEOPs [14,15], Dy5*B*O features a nonzero Cr XMCD signal opposing that of the other transition metal ions, hinting toward an overall ferrimagnetic order. Future studies involving neutron scattering techniques [5] combined with cryogenic magnetic imaging [44,45] might deepen the understanding of the exact magnetic structure of Dy5*B*O and the observed spin reorientation.

ACKNOWLEDGMENTS

F.S. is funded by the Swiss National Science Foundation (SNF) (Grant No. 200021_184684). Dy5BO film growth and structural characterization were performed at Aalto University. SQUID-VSM measurements were carried out on the Quantum Design MPMS3-137 device of the Laboratory for Mesoscopic Systems, ETH Zurich, Switzerland and the Laboratory for Multiscale Materials Experiments, Paul Scherrer Institute, Switzerland. We acknowledge the provision of facilities and technical support by Aalto University at OtaNano - Nanomicroscopy Center (Aalto-NMC).

[1] M. Fiebig, T. Lottermoser, D. Meier, and M. Trassin, Nat. Rev. Mater. **1**, 16046 (2016).

[2] J. M. D. Coey, M. Viret, and S. Von Molnár, Adv. Phys. **48**, 167 (1999).

[3] C. M. Rost, E. Sachet1, T. Borman, A. Moballegh, E. C. Dickey, D. Hou, J. L. Jones, S. Curtarolo, and J.-P. Maria, Nat. Commun. **6**, 8485 (2015).

[4] E. P. George, D. Raabe, and R. O. Ritchie, Nat. Rev. Mater. **4**, 515 (2019).

[5] A. R. Mazza, E. Skoropata, Y. Sharma, J. Lapano, T. W. Heitmann, B. L. Musico, V. Keppens, Z. Gai, J. W. Freeland, T. R. Charlton, M. Brahlek, A. Moreo, E. Dagotto, and T. Z. Ward, Adv. Sci. **9**, 2200391 (2022).

[6] D. Bérardan, S. Franger, D. Dragoe, A. Kumar Meena, N. Dragoe, Phys. Status Solidi RRL **10**, 328 (2016).

[7] P. A. Krawczyk, M. Jurczyszyn, J. Pawlak, W. Salamon, P. Baran, A. Kmita, L. Gondek, M. Sikora, C. Kapusta, and T. Straczek, J. Wyrwa, and A. Zywczak, ACS Appl. Electron. Mater. **2**, 3211 (2020).

[8] Y. Sharma, M.-C. Lee, K. C. Pitike, K. K. Mishra, Q. Zheng, X. Gao, B. L. Musico, A. R. Mazza, R. S. Katiyar, V. Keppens, M. Brahlek, D. A. Yarotski, R. P. Prasankumar, A. Chen, V. R. Cooper, and T. Z. Ward, ACS Appl. Mater. Interfaces **14**, 11962 (2022).

[9] J. L. Braun, C. M. Rost, M. Lim, A. Giri, D. H. Olson, G. N. Kotsonis, G.e Stan, D. W. Brenner, J.-P. Maria, and P. E. Hopkins, Adv. Mater. **30**, 1805004 (2018).

[10] Y. Sharma, Q. Zheng, A. R. Mazza, E. Skoropata, T. Heitmann, Z. Gai, B. Musico, P. F. Miceli, B. C. Sales, V. Keppens, M. Brahlek, and T. Z. Ward, Phys. Rev. Mater. **4**, 014404 (2020).

[11] Y. Sharma, B. L. Musico, X. Gao, C. Hua, A. F. May, A. Herklotz, A. Rastogi, D. Mandrus, J. Yan, H. N. Lee, M. F. Chisholm, V. Keppens, and T. Z. Ward, Phys. Rev. Mater. **2**, 060404(R) (2018).

[12] A. Kumar, D. Bérardan, D. Dragoe, E. Riviere, T. Takayama, H. Takagi, and N. Dragoe, Mater. Today Phys. **32**, 101026 (2023).

[13] R. Banerjee, S. Chatterjee, M. Ranjan, T. Bhattacharya, S. Mukherjee, S. S. Jana, A. Dwivedi, and T. Maiti, ACS Sustainable Chem. Eng. **8**, 17022 (2020).

[14] A. Farhan, F. Stramaglia, M. Cocconcelli, N. Kuznetsov, L. Yao, A. Kleibert, C. Piamonteze, and S. van Dijken, Phys. Rev. B **106**, L060404 (2022).

[15] A. Farhan, M. Cocconcelli, F. Stramaglia, N. Kuznetsov, L. Flajsman, M. Wyss, L. Yao, C. Piamonteze, and S. van Dijken, Phys. Rev. Mater. **7**, 044402 (2023).

[16] C. Ritter, R. Vilarinho, J. A. Moreira, M. Mihalik, M. Mihalik, and S. Savvin, J. Phys.: Condens. Matter **34**, 265801 (2022).

[17] B. Biswas, V. F. Michel, O. S. Fjellvåg, G. Bimashofer, M. Döbeli, M. Jambor, L. Keller, E. Müller, V. Ukleev, E. V. Pomjakushina, D. Singh, U. Stuhr, C. A. F. Vaz, T. Lippert, and C. W. Schneider, Phys. Rev. Mater. **6**, 074401 (2022).

[18] L. Hou, L. Shi, J. Zhao, S. Pan, Y. Xin, and X. Yuan, J. Phys. Chem. C **124**, 15399 (2020).

[19] C. Piamonteze, U. Flechsig, S. Rusponi, J. Dreiser, J. Heidler, M. Schmidt, R. Wetter, M. Calvi, T. Schmidt, H. Pruchova, J. Krempasky, C. Quitmann, H. Brune, and F. Nolting, J. Synchrotron Radiat. **19**, 661 (2012).

[20] Y.-L. Huang, D. Nikonov, C. Addiego, R. V. Chopdekar, B. Prasad, L. Zhang, J. Chatterjee, H.-J. Liu, A. Farhan, Y.-H. Chu, M. Yang, M. Ramesh, Z. Q. Qiu, B. D. Huey, C.-C. Lin, T. Gosavi, J. Íñiguez, J. Bokor, X. Pan, I. Young, L. W. Martin *et al.*, Nat. Commun. **11**, 2836 (2020).

[21] Y. Wu, J. Stohr, B. D. Hermsmeier, M. G. Samant, and D. Weller, Phys. Rev. Lett. **69**, 2307 (1992).

[22] See Supplemental Material http://link.aps.org/supplemental/10.1103/PhysRevB.109.134422 for further information on the XAS/XMCD fitting parameters and temperature-dependent magnetization measurements.

[23] E. Stavitski and F. M. De Groot, Micron **41**, 687 (2010)

[24] G. van der Laan, C. M. B. Henderson, R. A. D. Pattrick, S. S. Dhesi, P. F. Schofield, E. Dudzik, and D. J. Vaughan, Phys. Rev. B **59**, 4314 (1999).

[25] G. van der Laan, E. Arenholz, R. V. Chopdekar, and Y. Suzuki, Phys. Rev. B **77**, 064407 (2008).

[26] M. W. Haverkort, Z. Hu, J. C. Cezar, T. Burnus, H. Hartmann, M. Reuther, C. Zobel, T. Lorenz, A. Tanaka, N. B. Brookes, H. H. Hsieh, H.-J. Lin, C. T. Chen, and L. H. Tjeng, Phys. Rev. Lett. **97**, 176405 (2006).

[27] A. E. Bocquet, T. Mizokawa, K. Morikawa, A. Fujimori, S. R. Barman, K. Maiti, D. D. Sarma, Y. Tokura, and M. Onoda, Phys. Rev. B **53**, 1161 (1996).

[28] M. Abbate, F. M. F. de Groot, J. C. Fuggle, A. Fujimori, O. Strebel, F. Lopez, M. Domke, G. Kaindl, G. A. Sawatzky, M. Takano, Y. Takeda, H. Eisaki, and S. Uchida, Phys. Rev. B **46**, 4511 (1992).

[29] M. O. Krause and J. H. Oliver, J. Phys. Chem. Ref. Data **8**, 329 (1979).

[30] M. Y. Yang, S. Seong, E. Lee, M. Ghanathe, A. Kumar, S. M. Yusuf, K. Younghak, and J. S. Kang, Appl. Phys. Lett. **116**, 252401 (2020).

[31] B. Regmi, D. Miertschin, M. Cocconcelli, F. Stramaglia, D. Crater, L. Yao, C. Piamonteze, S. van Dijken, and A. Farhan, AIP Adv. **14**, 025023 (2024).

[32] H. Wang, H. Huang, Y. Feng, Y. C. Ku, C. E. Liu, S. Chen, A. Farhan, C. Piamonteze, Y. Lu, Y. Tang, J. Wei, L. Chen, C. F. Chang, C. Y. Kuo, and Z. Chen, ACS Appl. Mater. Interfaces**15**, **15** 58643 (2023).

[33] B. T. Thole, P. Carra, F. Sette, and G. van der Laan, Phys. Rev. Lett. **68**, 1943 (1992).

[34] P. Carra, B. T. Thole, M. Altarelli, and X. Wang, Phys. Rev. Lett. **70**, 694 (1993).

[35] C. T. Chen, Y. U. Idzerda, H.-J. Lin, N. V. Smith, G. Meigs, E. Chaban, G. H. Ho, E. Pellegrin, and F. Sette, Phys. Rev. Lett. **75**, 152 (1995).

[36] Y. Teramura, A. Tanaka, and T. Jo, J. Phys. Soc. Jpn. **65**, 1053 (1996).

[37] J. Dreiser, K. S. Pedersen, C. Piamonteze, S. Rusponi, Z. Salman, M. E. Ali, M. Schau-Magnussen, C. A. Thuesen, S. Piligkos, H. Weihe, H. Mutka, O. Waldmann, P. Oppeneer, J. Bendix, F. Nolting, and H. Brune, Chem. Sci. **3**, 1024 (2012).

[38] M. Yang, Q. Li, A. T. N'Diaye, Q. Y. Dong, N. Gao, E. Arenholz, C. Hwang, Y. Z. Wu, and Z. Q. Qiu, J. Magn. Magn. Mater. **460**, 6 (2018).

[39] A. Scholl, J. Stohr, J. Luning, J. W. Seo, J. Fompeyrine, H. Siegwart, J. Locquet, F. Nolting, S. Anders, E. E. Fullerton, M. R. Scheinfein, and H. A. Padmore, Science **287**, 1014 (2000).

[40] T. Zhao, A. Scholl, F. Zavaliche, K. Lee, M. Barry, A. Doran, M. P. Cruz, Y. H. Chu, C. Ederer, N. A. Spaldin, R. R. Das,

D. M. Kim, S. H. Baek, C. B. Eom, and R. Ramesh, Nat. Mater. **5**, 823 (2006).

[41] J. Li, E. Arenholz, Y. Meng, A. Tan, J. Park, E. Jin, H. Son, J. Wu, C. A. Jenkins, A. Scholl, H. W. Zhao, Chanyong Hwang, and Z. Q. Qiu, Phys. Rev. B **84**, 012406 (2011).

[42] Z. Y. Zhao, X. Zhao, H. D. Zhou, F. B. Zhang, Q. J. Li, C. Fan, X. F. Sun, and X. G. Li, Phys. Rev. B **89**, 224405 (2014).

[43] Y. Tokunaga, S. Iguchi, T. Arima, and Y. Tokura, Phys. Rev. Lett. **101**, 097205 (2008).

[44] M. Saccone, F. Caravelli, K. Hofhuis, S. Parchenko, Y. A. Birkhölzer, S. Dhuey, A. Kleibert, S. van Dijken, C. Nisoli, and A. Farhan, Nat. Phys. **18**, 517 (2022).

[45] A. Ullah, X. Li, Y. Jin, R. Pahari, L. Yue, X. Xu, B. Balasubramanian, D. J. Sellmyer, and R. Skomski, Phys. Rev. B **106**, 134430 (2022).